MOLECULAR LINE OBSERVATION TOWARD POLARIS FLARE

Seungyoup Chi and Yong-Sun Park
Astronomy Program, SEES, Seoul National University, Seoul 151-742, Korea
E-mail: csyoup@astro.snu.ac.kr

ABSTRACT

In an attempt to investigate star formation activity and statistical properties of clumps of high Galactic latitude clouds (HLCs), we mapped the Polaris Flare region, PF121.3+25.5, in ^{12}CO and ^{13}CO $J = 1 - 0$ using SRAO 6-m telescope and also observed its 12 ^{13}CO peak positions in CS $J = 2 - 1$ with TRAO 14-m telescope. ^{13}CO integrated intensity map shows clearly its clumpy structure and the locations of clumps well agree with ^{12}CO morphology. CS line is not detected toward the 12 ^{13}CO peak positions, so we can conclude there are no dense ($\sim 10^4$ cm^{-3}) in this region. We decomposed 105 clumps from ^{13}CO map using GAUSSCLUMPS algorithm. The mass of clumps ranges from 7.8 M$_\odot$ to 7.4×10^{-2} M$_\odot$ with a total mass of 66.4 M$_\odot$. The mass spectrum follows a power law, $dN/dM \propto M^{-\alpha}$ with a power index of $\alpha = 1.91 \pm 0.13$. The virial masses of clumps are in the range of $10 \sim 100$ M$_{LTE}$ and so these clumps are considered to be gravitationally unbound.

Key words : stars: formation—ISM: cloud—ISM: molecules—ISM: kinematics and dynamics

I. INTRODUCTION

For the past a few decades, surveys and studies on the star formation have been generally concentrated on the galactic plane due to its apparent star formation activities (Clemens & Barvainis 1988; Hartley *et al.* 1986; Lee *et al.* 1999; Lee *et al.* 2001; Myers *et al.* 1983). On the contrary, high Galactic latitude clouds (HLCs) are apparently inactive and subtend large angle, making it difficult to investigate in detail their structure and star formation activity. HLCs are commonly found to be gravitationally unbound because of their strong turbulent support against self-gravity. So, it has long been thought that HLCs are unable to form any stars (Magnani *et al.* 1985; de Vries *et al.* 1987; Heithausen 1996). Several T Tauri stars were discovered in a HLC, L1457 (MBM 12 in Magnani *et al.* 1985), but it is questionable whether L1457 is the parent cloud of these T Tauri stars.

However, there is at least one exception in a HLC, MCLD 123.5+24.9. This molecular cloud is located in the Polaris Flare, in the direction of the north celestial pole (Heithausen & Thaddeus 1990). The first molecular line observations toward MCLD 123.5+24.9 were carried out in ^{12}CO, ^{13}CO, OH, and H$_2$CO$^+$ (Groβmann *et al.* 1990) and this molecular cloud has been considered to be gravitationally unbound so far(Groβmann *et al.* 1990; Groβmann & Heithausen 1992; Boden & Heithausen 1993). After that, there have been both chemical and dynamical studies of this target. Heithausen (1999) observed dense cores embeded in MCLD 123.5+24.9, in CS (2−1), (3−2), and (5−4), finding that cores shows asymmetric double peaked line profiles which is known as an indication

of infall motion, prerequisite of star formation. In addition, Heithausen *et al.* (2002) found gravitationally bound cores in this HLC as the result of observations in HC$_3$N (3−2), (4−3), and (10−9). They show chemical structure indicating different evolutionary stages within the cloud. So, they suggested that even in gravitationally unbound clouds there can be locally gravitationally bound cores, possibly leading to star formation.

On the basis of these observational results for HLCs, in order to search for any star formation activity in other area, we conducted observational study toward a region named PF 121.3+25.5 in the the Polaris Flare which is adjacent to the well studied MCLD 123.5+24.9 (Fig.1). Its distance is between 130 pc and 240 pc (cf. Heithausen *et al.* 1993), and almost previous studies on this region use 150 pc. Therefore, we also adopt the distance of 150 pc in this paper. First, we carried out large area mapping observations in ^{12}CO and ^{13}CO. Additionally we observed in CS (J=2−1) the peak positions identified from the ^{13}CO map, for the purpose of searching for gravitationally bound clumps or dense cores under infall motion. Using these mapping observations, we will be able to find statistical properties of clumps such as mass spectrum as well. The observations in both Seoul Radio Astronomical Observatory (SRAO) and Taeduk Radio Astronomical Observatory (TRAO) are described in section II. The observational results are reported in section III. We present clump finding procedure and its results in section IV, and discussions are in section V.
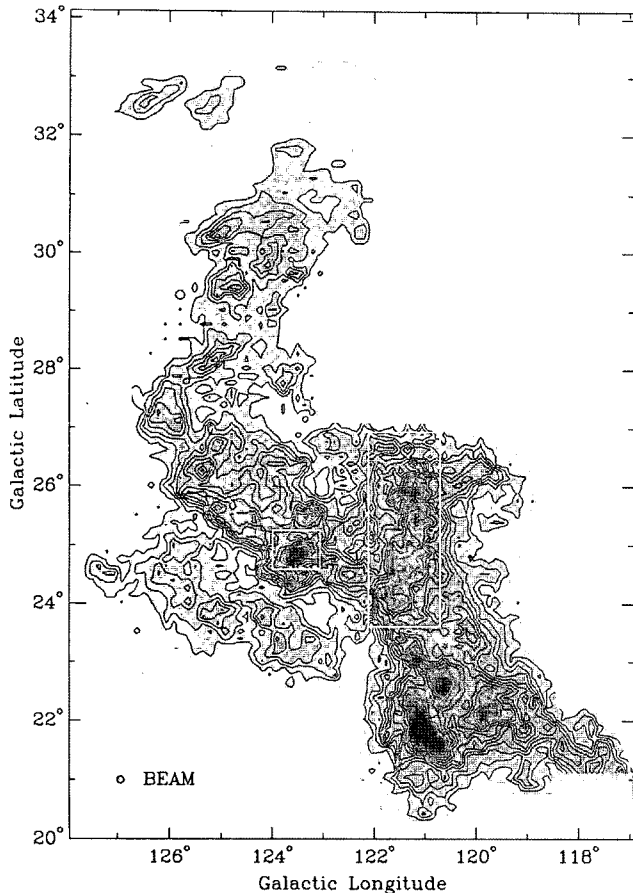

Corresponding Author: S. Chi

Fig. 1.— The mapping area of Polaris Flare. This figure indicates the velocity integrated ^{12}CO intensity map toward the Polaris Flare (Heithausen & Thaddaus 1990). The right white rectangle represents observed area in this paper and left rectangle is central part of MCLD 123.5+24.9.

II. MOLECULAR LINE OBSERVATION

(a) ^{12}CO and ^{13}CO Mapping

We carried out mapping observations in both ^{12}CO J=1−0 (115.271204 GHz) and ^{13}CO J=1−0 (110.201353 GHz) toward PF 121.3+25.5. These two observations are pilot mapping to decide the position of dense clumps, so we observed with higher spatial resolution than Heithausen & Thaddaus (1990). The observations were performed from December 2002 to May 2003 using SRAO 6-m telescope by frequency switching mode. First, we mapped about 2°× 3° area of the PF 121.3+25.5 region (Fig.1) in ^{12}CO with 4′ spacing and the r.m.s level of $\Delta T_R^* \sim 0.2$ K with 0.25 km s^{-1} spectral resolution. Then we observed in ^{13}CO transition a sub-region of about 2.5 deg^2 which is bright in ^{12}CO map. The mapping grid and sensitivity are 2′ and $\Delta T_R^* \sim 0.2$ K in the spectral resolution of 0.27 km s^{-1}, respectively.

The SRAO telescope has the beam size of 100″ and the main beam efficiency of 0.70 at 115GHz. The pointing accuracy is better than 10″ in both direction of azimuth and elevation. A 1024 channel auto-correlation spectrometer configured with a band width of 50 MHz was used for backend. The spectral resolution is 49 KHz or 0.127 km s^{-1} at the CO frequency (Koo et al. 2003). Data were calibrated using standard chopper wheel method.

(b) CS J=2−1 Line Observation

For the purpose of searching for gravitationally bound clumps or cores under infall motion, we observed 12 peak positions and several neighboring positions selected from ^{13}CO map in CS J=2−1 line (97.980968 GHz). The CS is known as one of high density tracers due to its high dipole moment. This observation was carried out using TRAO 14-m telescope for three weeks, between April and May 2003. The beam size of the telescope is 60″ and the main beam efficiency is 0.48 at 98 GHz. The pointing error is less than 10″ in both azimuth and elevation for all direction. We used a 1024 channel auto-correlator with spectral resolution of 10 kHz and chopper wheel calibration to obtain the antenna temperature, T_A^*. The observation was performed using frequency switching mode and the sensitivity is $0.05 \sim 0.09$ K.

III. OBSERVATIONAL RESULTS

We made the ^{12}CO and ^{13}CO J=1−0 maps for the PF 121.3+25.5 with 4′ and 2′ resolutions, respectively (Fig 2 and Fig 3). The peak temperature of ^{12}CO over the observed region is $T_A^* \sim 6.4$ K. The ^{12}CO lines in this region have several velocity components, of which range is from −7 to 0 km s^{-1}, and most of them are overlapped each other (Fig. 4). All of ^{12}CO spectra are contaminated by the telluric line, of which velocity is at −0.5 km s^{-1} (Fig. 5). Because of this contamination, we need to extract the contribution of telluric line in order to make total integrated intensity map of ^{12}CO. We simply subtracted the contribution of telluric line, which is estimated from several isolated lines. Such a method is valid because both intensity and width of telluric line remain almost constant.

The ^{13}CO integrated intensity map shows clearly its clumpy structure (Fig. 3) and the locations of clumps generally agree with the bright parts of ^{12}CO map. The velocity range of ^{13}CO components is between −5 and −2 km s^{-1}, but there are several positions of which velocity reaches down to about −10 km s^{-1} (Fig. 5). Telluric molecular line is invisible in ^{13}CO.

We also observed 12 peak positions of ^{13}CO map in CS J=2−1, but detected no CS emission. It seems to be that there are no dense ($\sim 10^4$ cm^{-3}) cores in this region. Therefore, from now on, we concentrate on describing decomposition of clumps identified from the
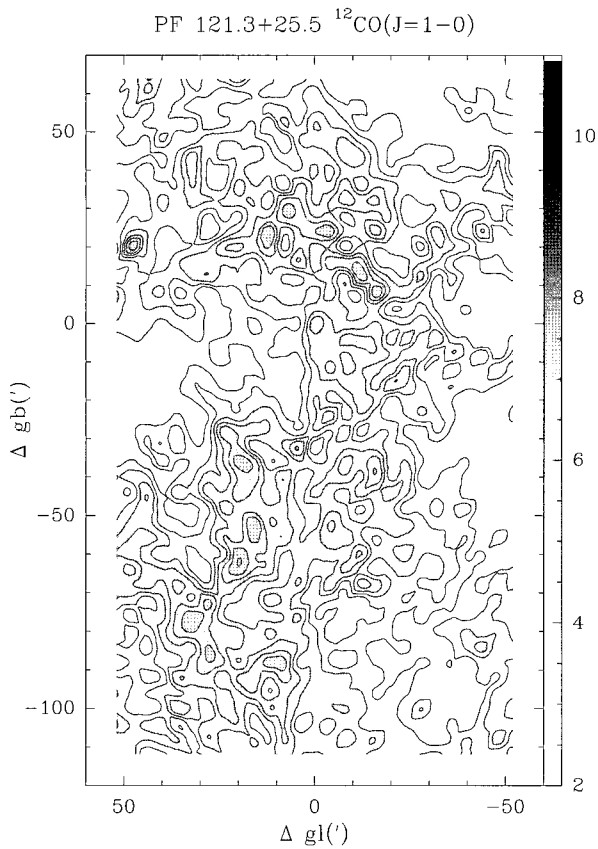
PF 121.3+25.5 ^{12}CO(J=1-0)

Fig. 2.— ^{12}CO integrated intensity map of PF121.3+25.5. The velocity range is between -7 and 1 km s^{-1}.

PF121.3+25.5 ^{13}CO(J=1-0)

Fig. 3.— ^{13}CO integrated intensity map of PF121.3+25.5. The velocity range is between -5 and 0 km s^{-1}.

^{13}CO data, and deriving their statistical properties like mass spectrum. Then stability analysis for decomposed clumps based on virial theorem follows.

IV. CLUMPS IDENTIFICATION AND MASS SPECTRUM

We carried out the decomposition of clumps from the ^{13}CO integrated intensity map. There are several methods for decomposing clumps in 3-dimensional space, i.e., position-position-velocity space. Among them, two algorithms, GAUSSCLUMPS (Stutzki & Güsten 1990) and CLUMPFIND (Williams et al. 1994), are generally known. Briefly speaking, GAUSSCLUMPS is the algorithm which finds the 3-dimensional Gaussian-shaped clumps by iteratively assigning a clump to the peak position in the map. On the other hand, CLUMPFIND algorithm operates on the 3-dimensional data in the same way as the eye would analyze a data set by using local maxima. In some case, CLUMPFIND misses low-mass clumps and makes a mass spectrum
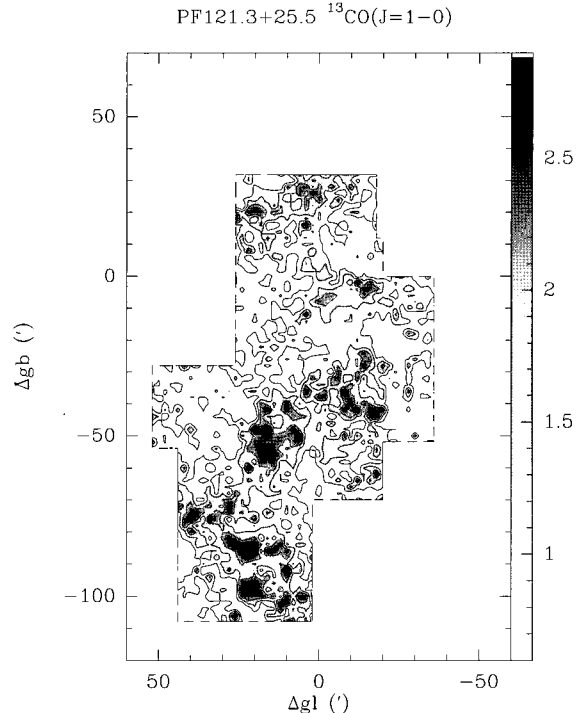
flatter at the low-mass end, whereas GAUSSCLUMPS tends to find more low-mass clumps. In practice, these two algorithms, however, agree well with each other. In this study, we used GAUSSCLUMPS because our sources are not so bright and, therefore, GAUSS-CLUMPS may be more effective. One more advantage is that this algorithm can work together with the data reduction package, GILDAS, that we are using. The GAUSSCLUMPS requires fully sampled data set, so we smoothed the data set with 4′ Gaussian beam.

As a result, we identified 128 clumps, but need to check misidentification. Because this algorithm forces the unresolved clumps to have a size corresponding to the spatial and velocity resolution, if all the 3-dimensional size of a clump is the same as resolutions in each axes, the clump may not be a real one. In this way, 23 clumps are proven to be false and ruled out. Finally 105 clumps are identified as listed in Table 1. To calculate the masses of the clumps from the fitted parameters, we derive ^{13}CO J=1$-$0 column density using the following formula and convert it into clumps mass. We assumed that the excitation temperature is $T_{ex} \sim 10$ K, distance to PF 121.3+25.5 is d ~ 150 pc, and the conversion factor between H$_2$ and ^{13}CO is $N(H_2) = 5.0 \times 10^5\ N(^{13}CO)$. It is also assumed that the ^{13}CO line is optically thin.
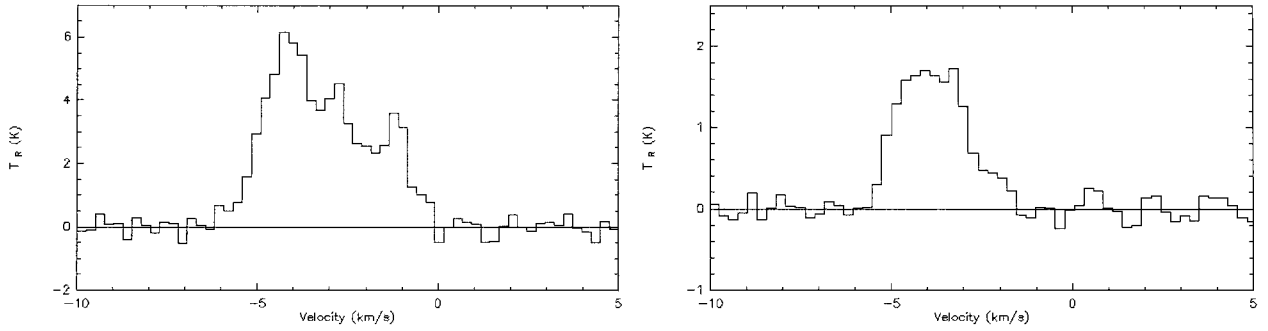
Fig. 4.— Line profiles of ^{12}CO (left) and ^{13}CO (right). These profiles are averaged over the central $10'$ region.
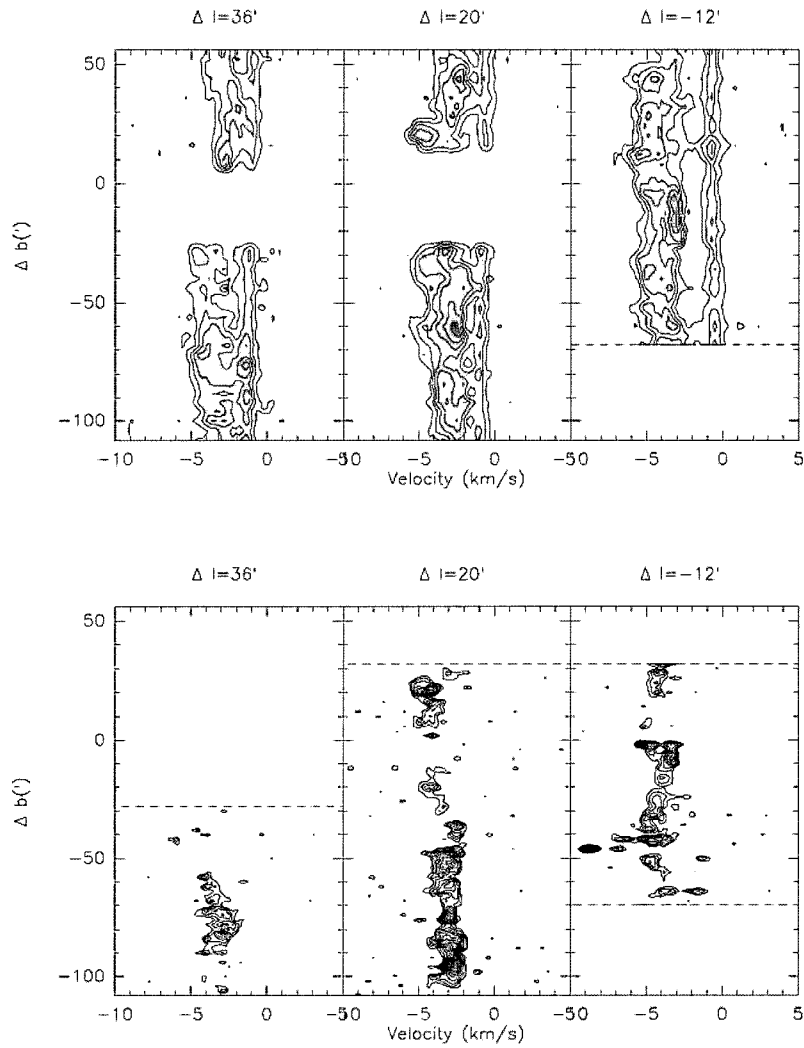

Fig. 5.— The position-velocity map of ^{12}CO (upper) and ^{13}CO (lower). Telluric component is shown at -0.5 km s^{-1} in the ^{12}CO map.

$$N_{total}^{13CO} = 2.422 \times 10^{14} \frac{T_{ex} \int \tau dv}{1 - exp\left[-5.3\middle/T_{ex}\right]} \quad (1)$$

$$M = m_{H_2} \frac{N(H_2)}{N(^{13}CO)} 2.422 \times 10^{14} \frac{\int \int T_{MB} dv dA}{1 - exp\left[-5.3\middle/T_{ex}\right]} \quad (2)$$

In terms of fitting parameters in Table 1, equation (2) can be recast in the following form,

$$M = T_{MB}(K) \times \Delta x('') \times \Delta y('') \times \Delta v(\mathrm{kms}^{-1})$$
$$\times 3.009 \times 10^{-6} \ M_{\odot} \quad (3)$$

Similarly, we can also calculate the lower mass limit that can be found by GAUSSCLUMPS.

$$M_{min}^{limit} \propto T_{rms} \times \Delta x_{beam} \times \Delta y_{beam} \times \Delta v_{res} = 0.013 \ M_{\odot} \quad (4)$$

The clump mass is found to range from 7.8 $M_{\odot}$ to 7.4 $\times$ 10^{-2} $M_{\odot}$ with a mean value of 6.8 $\times$ 10^{-1} $M_{\odot}$. The total mass of decomposed clumps is found to be 66.4 $M_{\odot}$. The mean size is 5.8'$\times$11.0' and the mean line width is 0.5 km s^{-1}. We derive the mass spectrum for the 105 clumps and plot it in Fig. 6. The mass spectrum can be approximated by a power law, $dN/dM \propto M^{-\alpha}$ with an index of $\alpha = 1.91 \pm 0.13$ for PF121.3+25.5. It has been known that the α ranges generally from 1.4 to 1.9 for Galactic plane clouds (see a review by Blitz 1993). Thus the value derived for PF121.3+25.5 is close to the upper limit.

V. DISCUSSION

We carried out the observation in CS J=2$-$1 molecular line, but failed to detect emission. With this result, one can estimate the upper limit of CS core mass. Assuming that we could identify the signal brighter than 3σ level and the excitation temperature is 5 K roughly, we applied an similar equation (Eq. 4) to this case. The resulting lower limit of CS core mass is estimated to be $M_{limit} \sim 4 \times 10^{-4}$ $M_{\odot}$. Therefore, in the region we observed in CS J=2$-$1 line, there seems to be no CS dense core which is more massive than $\sim 10^{-4}$ $M_{\odot}$.

We can also estimate the virial mass of each ^{13}CO clump using the following expression,

$$M_{vir} = \frac{5}{8ln2} \frac{R\Delta v^2}{G} = 9.134 \cdot \left(\frac{\Delta v}{kms^{-1}}\right)^2 \left(\frac{\Delta x}{arcmin}\right) M_{\odot} \quad (5)$$
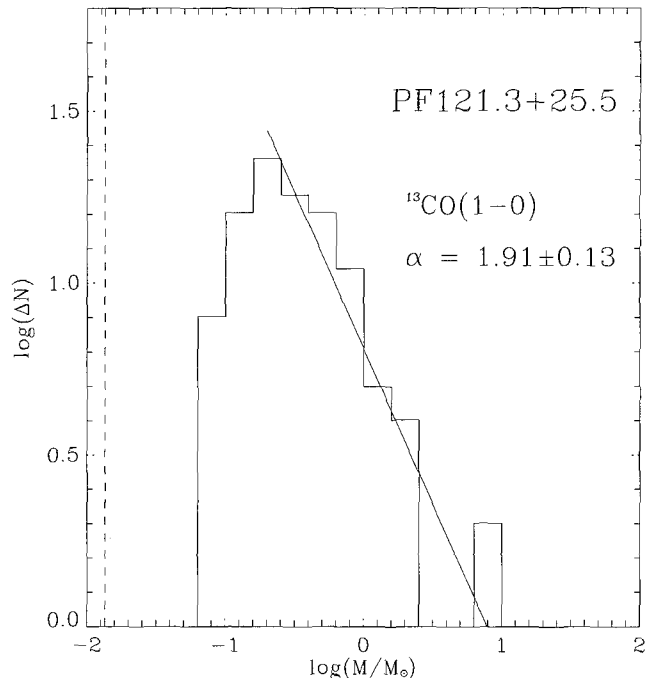

Fig. 6.— The mass spectrum of the ^{13}CO clumps. The solid line represents least square linear fit, and dashed line indicates lower limit of clump mass given by the resolution limit.

The virial masses, M_{vir}, derived in this way are compared with clump masses from LTE assumption in figure 7. It is found that the virial masses of almost all clumps are in the range of 10 $\sim$ 100M_{LTE}. Even if we consider the uncertainty in distance to the cloud, $M_{vir} \geq 5M_{LTE}$, which means any clumps are not virialized. It may be not surprising that there is no clumps under virial equilibrium, because ^{13}CO might not trace the compact core as in the case of MCLD 123.5+24.9.

There have been several previous studies on clumps mass spectrum and stellar initial mass function. Kramer et al. (1998) presented clump mass spectra of the several molecular clouds. Some of those clouds show the evidence of star-forming activities and others not yet. They found power law indices α lying between 1.6 and 1.8. On the other hand, Motte et al. (1998) presented the results of 1.3 mm continuum observation toward ρ Ophiuchi dark cloud, which is one of the most conspicuous region where low-mass star formation is taking place. They found power law mass spectrum with $\alpha \sim 1.5$ for the 0.1 $\sim$ 0.5 $M_{\odot}$, and $\alpha \sim 2.5$ for the 0.5 $\sim$ 3 $M_{\odot}$. These results well agree with stellar initial mass function, which is known to have $\alpha \sim 1.5$ for the lower mass stars, $M_* \leq 1$ $M_{\odot}$, and $\alpha \sim 2.5$ for higher mass stars, 1 $M_{\odot} \leq M_* \leq 10$ $M_{\odot}$ (Salpeter 1955, Güsten & Mezger 1983).

In conclusion, the PF 121.3+25.5 is thought to be

in a stage similar to that of objects in Kramer *et al.* (1998), but the power index of PF 121.3+25.5 is larger than that of these objects meaning that massive clumps are relatively rare in PF 121.3+25.5. Based on the fact that the more massive clumps are more likely to evolve to form stars, it seems that the PF 121.3+25.5 regions are not so efficient in star-forming.

VI. SUMMARY

We carried out ^{12}CO and ^{13}CO J=1−0 mapping observation using SRAO 6-m telescope toward a HLC in Polaris Flare, PF121.3+25.5. In addition, the peak positions revealed in ^{13}CO map are observed in CS J=2−1 with TRAO 14-m telescope. The main purpose of this observation is to search for gravitationally bound clumps or cores under infall motion which is evidence of star formation and to investigate the statistical properties of identified clumps. The main conclusions from this observational study are summarized below.

1. We presented the ^{12}CO map with 4 ′ spacing and ^{13}CO map with an angular resolution of 2′ for a HLC, PF121.3+25.5. The ^{13}CO map are show clearly its clumpy structure and the locations of clumps well agree with the ^{12}CO morphology.

2. In the CS J=2−1 observation toward 12 ^{13}CO peak positions, we could not detect any emissions suggestive of the existence of dense cores.

3. We decomposed clumps from ^{13}CO map with the 3-dimensional Gaussian fitting algorithm, GAUSS-CLUMPS and identified 105 clumps. The mass range of these clumps is from 7.8 $M_\odot$ to 7.4×10^{-2} $M_\odot$ and the total mass of the clumps is found to be $\sim$ 66.4 $M_\odot$.

4. The mass spectrum of clumps approximately follows a power law, $dN/dM \propto M^{-\alpha}$ with an index of $\alpha = 1.91 \pm 0.13$. In addition, the virial mass of clumps are in the range of 10∼100 M_{LTE}. Therefore, these clumps are considered to be gravitationally unbound.

REFERENCES

Boden, K. -P. & Heithausen, A., 1993, A Multi-Molecular Study of the Dense High-LatitudeCloud MCLD 126.6+24.5 A&A, 268, 255

Clemens, D. P. & Barvainis, R., 1988, A Catalog of Small, Optically Selected Molecular Clouds - Optical, Infrared, and Millimeter Properties, ApJS, 68, 257

de Vries, H. W., Heithausen, A., & Thaddeus, P., 1987, Molecular and Atomic Clouds Associated with Infrared Cirrus in Ursa Major, ApJ, 319, 723

Groβmann, V. & Heithausen, A., 1992, The Physical and Chemical State of a Dense Core in the High-Latitude Cloud MCLD 123.5 + 24.9, A&A, 264, 195

Groβmann, V., Heithausen, A., Meyerdierks, H., & Mebold, U., 1990, A High-Latitude Cloud with Increased Hydroxyl Abundance, A&A, 240, 400

Güsten, R. & Mezger, P. G., 1983, Star Formation and Abundance Gradients in the Galaxy, Vistas in Astronomy, 26, 159

Hartley, M., Manchester, R. N., Smith, R. M., Tritton, S. B., & Goss, W. M., 1986, A Catalogue of Southern Dark Clouds, A&AS, 63, 27

Heithausen, A., 1996, On the Dynamical State of High-Latitude Molecular clouds, A&A, 314, 251

Heithausen, A., 1999, Evidence for Inward Motion in a Galactic Cirrus Core, A&A, 349, L53

Heithausen, A., Bertoldi, F., & Bensch, F., 2002, Gravitationally Bound Cores in a Molecular Cirrus Cloud, A&A, 383, 591

Heithausen, A. Stacy, J. G., de Vries, H. W., Mebold, U., & Thaddeus, P., 1993, A Composite Large-Scale CO Survey at High Galactic Latitudes in the Second Quadrant, A&A, 268, 265

Heithausen, A. & Thaddeus, P., 1990, The Polaris Flare - Extensive Molecular Gas Near the North Celestial Pole, ApJ, 353, L49

Koo, B. -C., Park, Y. -S., Hong, S. S., Yun, H. -S., Lee, S. -G., Byun, D. -Y., Lee, J. -W., Choi, H. -K., Lee, S. -S., & Yoon, Y. -Z., 2003, Performance of the SRAO 6-Meter Radio Telescope, JKAS, 36, 43
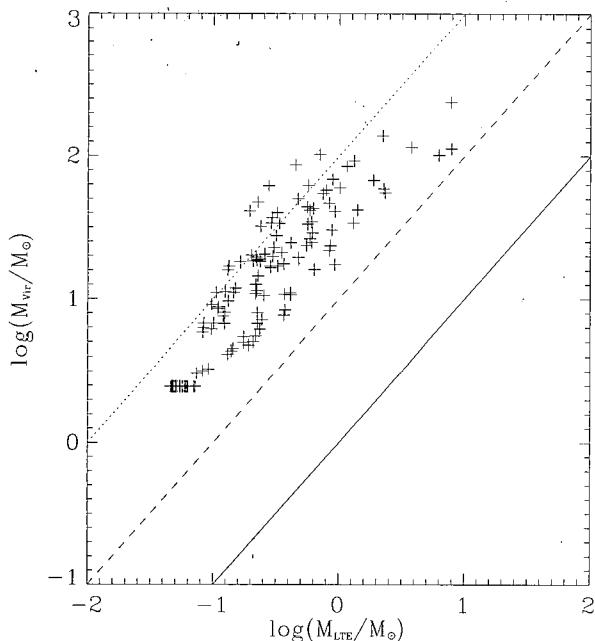
Fig. 7.— The relation between M_{LTE} and M_{vir} of ^{13}CO clumps. The solid line represents $M_{vir} \sim M_{LTE}$, dashed line is for $M_{vir} \sim 10M_{LTE}$, and dotted line is for $M_{vir} \sim 100M_{LTE}$.

Kramer, C., Stutzki, J., Röhrig, R., & Corneliussen, U., 1998, Clump Mass Spectra of Molecular Clouds, A&A, 329, 249

Lee, C. W., Myers, P. C., & Tafalla, M., 1999, A Survey of Infall Motions toward Starless Cores. I. CS(2-1) and N_2H^+(1-0) Observations, ApJ, 526, 788

Lee, C. W., Myers, P. C., & Tafalla, M., 2001, A Survey for Infall Motions toward Starless Cores. II. CS(2-1) and N_2H^+(1-0) Mapping Observations, ApJS, 136, 703

Magnani, L., Blitz, L., & Mundy, L., 1985, Molecular Gas at High Galactic Latitudes, ApJ, 295, 402

Motte, F., André, P., & Neri, R., 1998, The initial Conditions of Star Formation in the Rho Ophiuchi Main Cloud: Wide-Field Millimeter Continuum Mapping, A&A, 336, 150

Myers, P. C., Linke, R., & Benson, P. J., 1983, Dense Cores in Dark Clouds. I - CO Observations and Column Densities of High-Extinction Regions, ApJ, 264, 517

Salpeter, E. E., 1955, The Luminosity Function and Stellar Evolution, ApJ, 121, 161

Stuzki, J. & Güsten, R., 1990, High Spatial Resolution Isotopic CO and CS Observations of M17 SW - The clumpy Structure of the Molecular Cloud Core, ApJ, 356, 513

Williams, J. P., de Geus, E. J., & Blitz, L., 1994, Determining Structure in Molecular Clouds, ApJ, 428, 693

TABLE 1
LIST OF 105 CLUMPS

Clump ID	Δgl $(')^{a}$	Δgb $(')^{a}$	v (kms^{-1})	$T_b(K)$	Δx $(')^{b}$	Δy $(')^{b}$	Δv $(kms^{-1})^{b}$	Mass $(M_{\odot})$
1	17.9	−54.0	−3.27	3.10	9.70	23.30	0.82	6.22E+00
2	24.0	−98.0	−2.47	2.61	6.30	84.60	0.52	7.84E+00
3	−4.0	−8.0	−3.27	2.22	6.40	13.40	0.68	1.40E+00
4	4.0	−36.0	−4.60	2.16	14.80	4.30	0.59	8.79E−01
5	16.1	−94.1	−2.47	2.17	5.90	65.90	0.85	7.77E+00
6	8.0	−86.0	−3.00	2.08	4.00	8.00	0.78	5.62E−01
7	12.0	20.0	−4.07	2.07	25.70	7.50	0.87	3.76E+00
8	40.0	−80.0	−2.74	2.01	4.00	12.50	1.06	1.15E+00
9	10.0	−108.0	−2.47	1.93	4.50	49.20	0.49	2.27E+00
10	10.0	−92.0	−3.27	1.74	63.90	4.60	0.42	2.33E+00
11	−14.0	−4.0	−3.80	1.72	6.30	22.20	0.72	1.88E+00
12	4.0	4.0	−3.53	1.72	6.00	11.70	0.71	9.29E−01
13	10.0	28.0	−4.60	1.69	4.00	30.80	0.37	8.35E−01
14	24.0	−98.0	−3.00	1.68	4.00	8.10	0.38	2.24E−01
15	−18.0	−44.0	−4.07	1.67	4.00	35.00	0.88	2.23E+00
16	−8.0	−36.0	−5.66	1.69	4.00	4.00	1.54	4.51E−01
17	28.0	18.0	−4.33	1.64	4.40	4.50	0.67	2.36E−01
18	4.0	−12.0	−4.60	1.63	4.90	9.70	0.72	6.04E−01
19	22.0	−60.0	−4.33	1.61	4.00	6.20	0.70	3.03E−01
20	6.0	−50.0	−3.80	1.60	6.70	9.80	0.89	1.01E+00
21	38.0	−74.0	−2.21	1.61	4.40	4.00	0.94	2.89E−01
22	−14.0	−4.0	−4.60	1.57	4.00	52.20	0.26	9.23E−01
23	28.0	−92.0	−2.21	1.58	4.50	4.00	0.71	2.19E−01
24	14.0	−80.0	−3.27	1.55	20.90	4.00	0.26	3.65E−01
25	2.0	30.0	−3.80	1.54	4.00	14.30	0.83	7.92E−01
26	28.0	−72.0	−4.07	1.53	4.00	7.60	1.39	7.00E−01
27	18.0	−44.0	−2.74	1.55	4.00	16.50	0.53	5.87E−01
28	−20.0	−42.0	−4.86	1.53	4.00	6.10	0.56	2.27E−01
29	0.0	−38.0	−4.60	1.50	4.00	12.30	0.26	2.08E−01
30	−12.0	−46.0	−8.85	1.52	4.00	4.00	0.55	1.45E−01
31	20.0	−84.0	−2.21	1.49	4.00	11.40	0.26	1.91E−01
32	16.0	−48.0	−2.21	1.48	4.00	16.10	0.46	4.75E−01
33	46.0	−72.0	−3.27	1.46	15.50	4.80	0.71	8.35E−01
34	−12.0	−2.0	−5.13	1.45	4.00	8.40	0.54	2.85E−01
35	−12.0	−42.0	−4.07	1.44	4.00	25.40	0.83	1.32E+00
36	−24.0	2.0	−3.27	1.43	4.00	23.10	0.26	3.72E−01
37	14.0	−56.0	−2.74	1.43	5.20	21.90	0.36	6.35E−01
38	−6.0	−30.0	−4.60	1.42	7.70	22.00	0.50	1.30E+00
39	−10.0	28.0	−4.33	1.41	4.40	15.00	0.88	8.87E−01
40	16.0	−86.0	−3.80	1.40	4.00	10.40	0.40	2.52E−01
41	−8.0	−52.0	−4.60	1.40	4.70	12.60	0.83	7.45E−01
42	6.0	−72.0	−3.80	1.39	10.80	4.00	0.50	3.25E−01
43	24.0	−74.0	−2.74	1.39	4.00	6.70	0.83	3.35E−01
44	26.0	−106.0	−1.67	1.40	4.00	13.80	0.26	2.18E−01
45	24.0	−86.0	−3.27	1.36	4.00	5.20	0.40	1.23E−01
46	22.0	−98.0	−2.21	1.36	4.00	4.00	0.41	9.66E−02
47	−18.0	−44.0	−3.27	1.35	4.00	4.00	0.43	1.01E−01
48	12.0	−82.0	−3.00	1.34	4.00	5.50	0.65	2.08E−01
49	−34.0	−6.0	−2.47	1.35	4.50	10.50	0.60	4.15E−01
50	0.0	−88.0	−2.74	1.32	4.00	4.10	0.70	1.64E−01
51	26.0	−106.0	−3.80	1.31	4.00	15.90	0.26	2.35E−01
52	22.0	20.0	−4.86	1.29	8.00	4.00	0.71	3.18E−01
53	−14.0	−40.0	−7.52	1.29	4.00	4.00	0.49	1.10E−01
54	22.0	−36.0	−2.21	1.29	9.30	4.00	0.57	2.96E−01
55	−18.0	−4.0	−4.60	1.28	4.00	4.10	0.48	1.09E−01
56	−4.0	−40.0	−4.33	1.27	4.00	9.50	0.90	4.71E−01
57	22.0	8.0	−4.60	1.27	16.90	4.00	0.67	6.23E−01
58	2.0	26.0	−4.86	1.27	8.60	15.70	0.46	8.54E−01

TABLE 1—*Continued*

Clump ID	Δgl (')[a]	Δgb (')[a]	v (kms^{-1})	$T_b(K)$	Δx (')[b]	Δy (')[b]	Δv (kms^{-1})[b]	Mass $(M_\odot)$
59	−2.0	−58.0	−4.33	1.25	11.10	4.00	0.95	5.71E−01
60	10.0	−42.0	−4.07	1.26	4.00	4.90	0.89	2.38E−01
61	10.0	−92.0	−3.80	1.26	4.00	8.50	0.47	2.18E−01
62	26.0	−82.0	−3.27	1.23	4.00	6.60	0.26	9.15E−02
63	16.0	−6.0	−3.80	1.24	4.00	26.80	0.42	6.05E−01
64	4.0	16.0	−4.07	1.22	4.00	4.00	1.30	2.75E−01
65	24.0	−50.0	−2.74	1.23	9.40	4.00	0.26	1.30E−01
66	2.0	8.0	−3.80	1.22	4.00	10.10	0.26	1.39E−01
67	32.0	−88.0	−3.00	1.20	4.00	30.50	0.26	4.12E−01
68	−30.0	2.0	−8.59	1.21	4.00	4.40	0.54	1.25E−01
69	−16.0	6.0	−5.40	1.19	4.00	4.00	0.40	8.25E−02
70	10.0	−74.0	−3.53	1.19	4.00	5.60	0.52	1.50E−01
71	−14.0	−6.0	−3.27	1.19	4.00	25.90	0.46	6.14E−01
72	18.0	−100.0	−3.27	1.20	4.00	10.60	0.26	1.43E−01
73	16.0	−100.0	−2.47	1.16	6.30	4.00	0.26	8.23E−02
74	−10.0	−44.0	−3.53	1.16	4.00	26.70	0.41	5.50E−01
75	−2.0	−12.0	−4.86	1.14	4.00	4.00	1.14	2.25E−01
76	0.0	−46.0	−3.27	1.14	4.00	13.60	0.26	1.75E−01
77	−6.0	24.0	−4.86	1.13	4.00	19.10	0.26	2.43E−01
78	2.0	26.0	−3.53	1.13	4.00	7.70	0.59	2.22E−01
79	−16.0	−46.0	−4.86	1.15	4.00	31.70	0.26	4.11E−01
80	30.0	−64.0	−4.07	1.13	4.00	12.10	0.48	2.84E−01
81	14.0	−22.0	−4.60	1.15	7.20	8.60	0.76	5.86E−01
82	24.0	−48.0	−2.47	1.12	4.00	4.20	0.41	8.36E−02
83	10.0	−92.0	−2.21	1.12	4.00	4.00	0.50	9.71E−02
84	30.0	−108.0	−3.00	1.12	4.00	14.40	0.50	3.49E−01
85	4.0	−100.0	−4.07	1.14	4.00	4.00	0.66	1.30E−01
86	46.0	−72.0	−2.47	1.12	4.00	17.80	0.26	2.25E−01
87	26.0	−82.0	−3.80	1.11	4.00	4.00	0.55	1.06E−01
88	−16.0	−60.0	−4.07	1.13	4.00	8.30	0.58	2.36E−01
89	14.0	−80.0	−3.53	1.11	5.90	4.00	0.26	7.38E−02
90	10.0	−92.0	−4.60	1.13	4.00	4.00	0.68	1.33E−01
91	10.0	−108.0	−3.80	1.10	4.00	6.00	0.46	1.32E−01
92	4.0	−102.0	−7.26	1.13	4.00	4.00	0.43	8.42E−02
93	32.0	−70.0	−3.00	1.11	4.00	11.60	0.39	2.18E−01
94	0.0	10.0	−4.33	1.10	4.00	11.60	0.40	2.21E−01
95	42.0	−60.0	−3.53	1.10	11.00	5.10	0.26	1.74E−01
96	42.0	−26.0	−2.21	1.07	4.00	6.80	0.64	2.02E−01
97	−12.0	−42.0	−5.13	1.06	4.00	30.80	0.26	3.68E−01
98	20.0	22.0	−3.80	1.07	4.00	6.50	0.41	1.24E−01
99	24.0	−26.0	−3.80	1.08	18.10	4.00	0.66	5.59E−01
100	36.0	−84.0	−3.80	1.05	4.00	20.00	0.40	3.64E−01
101	8.0	−108.0	−3.00	1.03	4.00	6.90	0.39	1.20E−01
102	14.0	8.0	−4.60	1.05	4.00	8.40	0.84	3.21E−01
103	22.0	2.0	−3.80	1.06	4.00	4.00	1.06	1.95E−01
104	0.0	−92.0	−3.80	1.05	4.60	6.60	0.85	2.94E−01
105	46.0	−68.0	−3.27	1.06	4.00	9.80	0.57	2.57E−01

[a] relative position in the map

[b] the size along each axis